Non-activation synthesis and thermodynamic properties of ternary compounds of the Ag–Te–Br system

Moroz, Mykola; Tesfaye, Fiseha; Demchenko, Pavlo; Prokhorenko, Myroslava; Prokhorenko, Serhiy; Reshetnyak, Oleksandr

Published in:
Thermochimica Acta

DOI:
10.1016/j.tca.2021.178862

Published: 01/04/2021

Document Version
Accepted author manuscript

Document License
CC BY-NC-ND

Non-activation synthesis and thermodynamic properties of ternary compounds of the Ag–Te–Br system

Mykola Moroz [a, b, *], Fiseha Tesfaye [c], Pavlo Demchenko [d], Myroslava Prokhorenko [e], Serhiy Prokhorenko [f], Oleksandr Reshetnyak [b]

[a] *Department of Chemistry and Physics, National University of Water and Environmental Engineering, 33028 Rivne, Ukraine*

[b] *Department of Physical and Colloid Chemistry, Ivan Franko National University of Lviv, 79005 Lviv, Ukraine*

[c] *Johan Gadolin Process Chemistry Centre, Åbo Akademi University, 20500 Turku, Finland*

[d] *Department of Inorganic Chemistry, Ivan Franko National University of Lviv, 79005 Lviv, Ukraine*

[e] *Department of Cartography and Geospatial Modeling, Lviv Polytechnic National University, 79013 Lviv, Ukraine*

[f] *Department of Measuring Information Technologies, Lviv Polytechnic National University, 79013 Lviv, Ukraine*

[*] Corresponding author. E-mail address: m.v.moroz@nuwm.edu.ua

Abstract

The division of the concentration space AgBr–Ag_2Te–Te **(I)**, which is a part of the Ag–Te–Br system, into 10 three-phase regions was established based on literature data and the results of the electromotive force (EMF) measurements in this work. The overall potential-forming reactions were expressed for the phase regions AgBr–$Ag_{19}Te_6Br_7$–Te, $Ag_{19}Te_6Br_7$–Ag_3TeBr–Te, Ag_3TeBr–$Ag_{10}Te_4Br_3$–Te, Ag_3TeBr–Ag_5Te_2Br–$Ag_{10}Te_4Br_3$, Ag_5Te_2Br–Ag_2Te–$Ag_{23}Te_{12}Br$, and $Ag_{10}Te_4Br_3$–$Ag_{23}Te_{12}Br$–Te. Reactions were performed by applying electrochemical cells (ECCs) of the type (−) IE | Ag | Solid-state electrolyte | R(Ag^+) | PE | IE (+), where IE is the inert electrode (graphite), Ag is the negative (left) electrode, PE is the positive (right) electrode, R(Ag^+) is the region of Ag^+ diffusion into PE. PEs of ECCs were prepared from finely ground mixtures of pure substances Ag, Te, and AgBr. The component ratios were determined from the equations of the potential-forming reactions in respective phase regions. Non-activation synthesis of the equilibrium set of phases was performed in the R(Ag^+) region of ECCs. The Ag^+ ions migrated from the left electrode to the right one for thermodynamic reasons act as nucleation centers for the equilibrium set of phases. The synthesis duration for the mixture particle size ~5 μm and T=500 K is under ≤5 hr. Linear dependences EMF vs T of ECCs between T=(440 and 500) K were used for calculations of the standard values of the Gibbs energies, enthalpies, and entropies of equilibrium compounds in **(I)**

consisting of $Ag_{19}Te_6Br_7$, Ag_3TeBr, $Ag_{10}Te_4Br_3$, Ag_5Te_2Br, and $Ag_{23}Te_{12}Br$. The observed experimental results and thermodynamic calculations are in good agreement.

Keywords: non-activation synthesis; thermoelectric materials; electromotive force method; Gibbs energy; thermodynamic functions.

1. Introduction

New energy materials discoveries enable various opportunities to meet the ever-increasing demand to produce cleaner energy. For the clean energy production through thermoelectric applications, new materials discoveries often aim at achieving higher figure of merit *ZT*, which is often used as measure of their performance, and a wider thermal stability ranges [1–3]. Multicomponent phases in the Ag–Te–Br system are among the class of materials under investigation as candidates for high performing thermoelectric materials. For instance, the study of Nilges et al. [4] on the Seebeck effect of the compound $Ag_{10}Te_4Br_3$ has resulted in interesting fluctuations with changing temperature.

The Ag–Te–Br system in the AgBr–Ag_2Te–Te **(I)** part features the formation of ternary compounds $Ag_{19}Te_6Br_7$ [5], Ag_3TeBr [6], Ag_5Te_2Br [7,8], $Ag_{10}Te_4Br_3$ [9,10], and $Ag_{23}Te_{12}Br$ [11,12]. The $Ag_{19}Te_6Br_7$, $Ag_{10}Te_4Br_3$, and $Ag_{23}Te_{12}Br$ compounds were obtained by melting appropriately weighed mixtures of Ag, Te, and AgBr at $T \leq 1270$ K for 1 day, followed by homogenizing annealing in the range of T=(620–663) K for 2-3 weeks. The Ag_3TeBr compound forms at T=710 K in the peritectic reaction $L + Ag_2Te = Ag_3TeBr$ [6]. An attempt to synthesis Ag_5Te_2Br compound in an evacuated quartz glass ampoules by [7] was not successful. They reported that the melt mixture of Ag : Te : AgBr = 4 : 2 : 1 resulted in two separate phases Ag_2Te and AgBr up on cooling to T=290 K. The Ag_5Te_2Br synthesis was achieved in an autoclave from the Ag_2Te and AgBr mixture in 12.5% aqueous ammonia at T=453 K over 14 days [7].

The crystal structures, electric conductivity, thermal conductivity, thermo-EMF, and heat capacity of the ternary compounds were investigated by some researchers [2,4,11–13]. The formation in cation and anion sub-lattices of low-dimensional spatially-oriented structural units with partially covalent bonding was established. The interaction of low-dimensional structural units depends strongly on temperature, e.g. temperature change of 4-morphic $Ag_{10}Te_4Br_3$ in the vicinity of T=390 K causes reversible switching between *p*- and *n*-type conduction. It accompanied by a huge jump of the Seebeck coefficient [4]. $Ag_{19}Te_6Br_7$ and $Ag_{23}Te_{12}Br$ exhibit similar properties [11]. A new approach to improving thermoelectric properties by generating low-dimensional interactions in solids was conceptualized in [2,13].

Thermodynamic properties of the Ag_3TeBr compound were determined by the electromotive force (EMF) method in [14]. No information on the thermodynamic properties of other ternary compounds of the Ag–Te–Br system was found.

The main objective of this work was to demonstrate the capabilities of non-activation synthesis of compounds in the Ag–Te–Br system where the energy of the thermal motion of atoms is insufficient for the formation of the nucleation centers of phases, and to determine thermodynamic properties of the ternary compounds of the system using EMF method. The results can be used in CALPHAD modeling [15] of the behavior of the ternary compounds in four-element space under substitutions Te → S, Se; Br → Cl, I.

2. Experimental

All substances used in this investigation are compiled in Table 1 together with their corresponding purity.

Table 1. Provenance and purity of materials used in the experiments. Purification and purity analysis methods are as stated by the supplier.

Chemical formula	Source	CAS No	Form	Mass fraction of purity
Ag	Sigma-Aldrich (Germany)	7440-22-4	Powder	0.9999
Te	Sigma-Aldrich (Germany)	13494-80-9	Powder	0.99999
AgBr	Lenreactiv (Russia)	7785-23-1	Powder	0.999
Ge	Lenreactiv (Russia)	7440-56-4	Powder	0.9999
S	Lenreactiv (Russia)	7404-34-9	Powder	0.9999
Ag_2GeS_3 [a]	Synthesis	–	Ingot	0.99

[a] Glassy material.

For the EMF measurements [16–21], the following electrochemical cells (ECCs) were assembled:

(−) IE | Ag | Solid-state electrolyte | R(Ag^+) | PE | IE (+), (A)

where IE is the inert electrode (graphite), Ag is the negative (left) electrode, PE is the positive (right) electrode, R(Ag^+) is the region of Ag^+ diffusion into PE.

A layout of the ECC is depicted in Fig. 1.

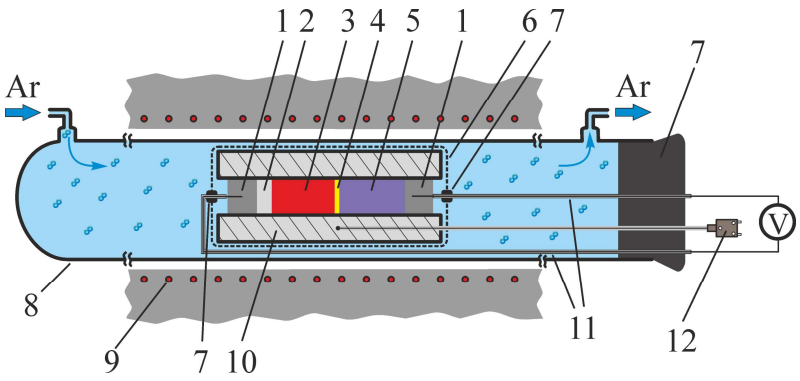

Fig. 1. Schematic illustration of the ECC for the EMF measurements in a horizontal furnace: graphite (1), left electrode (2), solid-state electrolyte (3), R(Ag^+) region (4), right electrode (5), aluminum shield (6), cork (7), quartz glass tube (8), furnace heater (9), fluoroplast matrix (10), current electrodes (11), and thermocouple (12).

Pure silver powder was used as a negative electrode. Ag_2GeS_3 glass was used as the solid-state electrolyte with purely Ag^+ ionic conductivity [22,23]. The Ag_2GeS_3 glass [22,24,25] was obtained by melt quenching of the corresponding elements from T=1200 K into ice water. Based on the high purity of the starting elements and good agreement of the glass transition and crystallization temperatures obtained in our study [25] with values reported in [22], we conclude that the purity of the synthesized glass is at least 0.99 mass fraction.

PE at the stage of the cell preparation is a well-mixed composition of finely ground mixtures of pure substances Ag, Te, and AgBr, with particle size ~5 μm. The ratios of the elements and the compound were determined from the equations of the potential-forming reactions in respective phase regions. ECC components in powder form were pressed at 10^8 Pa through a 2 mm diameter hole arranged in the fluoroplast matrix up to density $\rho = (0.93 \pm 0.02)\cdot\rho_0$, where ρ_0 is the experimentally determined density of cast samples [26]. The process of forming the equilibrium set of phases in the R(Ag^+) region for the particle size of the heterogeneous phase mixture ~5 μm and T=500 K took less than 5 h. The criterion for completing the formation of the equilibrium set of phases is the reproducibility of the EMF vs T dependences of ECCs during the heating-cooling cycles. Due to their amount in the scale of ppm, it was technically challenging to obtain the equilibrium set of phases from the pressed components of ECCs for X-ray diffraction analysis, similar to the case in [27].

EMF measurements were performed in a horizontal resistance furnace, similar to that described in [28]. As protective atmosphere, we used a continuously flowing highly purified (0.9999 volume fraction) Ar(g) at $P = 1.2\cdot10^5$ Pa, with a flow rate of $2\cdot10^{-3}$ $m^3\cdot h^{-1}$ from the left to right electrode of the ECCs. The temperature was maintained with an accuracy of ±0.5 K. The EMF

(E) of the cells were measured by high-resistance (input impedance of $>10^{12}$ Ω) universal U7-9 digital voltmeter. The heating and cooling rates were 2 K·min^{-1}. In our previous works [29,30] we have described the scheme of ECCs and procedure of the EMF measurements.

3. Results and discussion

In ECCs of type (A), the left electrode contains powdered silver, and the right one contains a powdered mixture of Ag, Te, and AgBr. According to the phase diagram of the Ag–Te system [31], silver and tellurium are not in equilibrium with each other. The presence of EMF in newly assembled ECCs was established. The EMF of the cells changes uncontrollably in the range of ± 1.5 mV at T = 300 K. The EMF changes are only due to the diffusion of Ag^+ ions through the solid-state electrolyte of ECCs. EMF fluctuations disappear when the cells are heated at a rate of 3–4 K·min^{-1} up to temperatures of 380–400 K. With subsequent heating, the initial value of the EMF increases by 3–5 mV·min^{-1}. The time to reach the value E = const of the cells at the isothermal annealing temperature T=500 K does not exceed 5 h.

One of the possible explanations for the presence of EMF of cells, its influence on the decay of metastable phases and the formation of equilibrium set of phases is as follows: at certain points in time at T > 380 K, nanoscale sections of PE are characterized by the vibrational energy of silver and tellurium atoms significantly exceeding kT (k is the Boltzmann Constant). This energy, together with the surface energy of silver particles, is sufficient to interact with tellurium. The result of this interaction is the formation of silver tellurides films of undetermined composition on the silver surface. In this case, the positive electrode contains a metastable set of phases from tellurium, silver tellurides, and silver bromide. The difference in the chemical potentials of silver in the ECC electrodes causes the displacement of Ag^+ ions from the left to the right electrode, i.e. EMF formation. Ag^+ ions are not a phase and do not chemically interact with the PE components. They play the role of a small nucleus of a stable phase [32]. Positive charges Ag^+ are held in the R(Ag^+) region by the forces of Coulomb attraction with negative charges of the left electrode. The presence of a positive charge in the R(Ag^+) region is an important condition for low-temperature non-activation synthesis of the equilibrium set of phases. The positive spatial charge reduces the forces of Coulomb repulsion between the metastable components of the PE. Under these conditions, the energy of the thermal motion of the PE components is sufficient to bring them closer to the distance of the action of the forces of chemical interaction. Thus, individual Ag^+ ions and the total positive charge in the R(Ag^+) region provide non-activation decomposition of the metastable phases and formation of the equilibrium set of phases.

The described model of non-activating synthesis of the equilibrium set of phases in the ECC is based on the following experimental positions:

a) the time to reach a constant EMF value in the ECC at T=500 K is ≤5 h;

b) the calculated values of the Gibbs energy of formation of the $Ag_{23}Te_{12}Br$ compound in the two adjacent phase regions coincide within the experimental error.

The concentration space of the Ag–Te–Br system in the part **(I)** consists of 10 three-phase regions listed in Table 2. These regions are marked out by the lines of two-phase equilibria in Fig. 2.

Table 2. Three-phase regions in the $AgBr–Ag_2Te–Te$ part and the respective EMF values of ECCs in corresponding phase regions at T=460 K [a].

Number of the phase region	Phase region	E / mV
PR(1)	$AgBr–Ag_{19}Te_6Br_7–Te$	238.86
PR(2)	$Ag_{19}Te_6Br_7–Ag_3TeBr–Te$	235.22
PR(3)	$Ag_3TeBr–Ag_{10}Te_4Br_3–Te$	231.43
PR(4)	$Ag_3TeBr–Ag_5Te_2Br–Ag_{10}Te_4Br_3$	201.72
PR(5)	$Ag_5Te_2Br–Ag_2Te–Ag_{23}Te_{12}Br$	200.42
PR(6)	$Ag_{10}Te_4Br_3–Ag_{23}Te_{12}Br–Te$	230.11
PR(7)	$Ag_5Te_2Br–Ag_{23}Te_{12}Br–Ag_{10}Te_4Br_3$	244.83
PR(8)	$Ag_{23}Te_{12}Br–Ag_5Te_3–Te$	–
PR(9)	$Ag_{23}Te_{12}Br–Ag_{1.9}Te–Ag_5Te_3$	–
PR(10)	$Ag_{23}Te_{12}Br–Ag_2Te–Ag_{1.9}Te$	–

[a] Standard uncertainties u are $u(T)$=0.1 K, $u(E)$=0.3 mV.

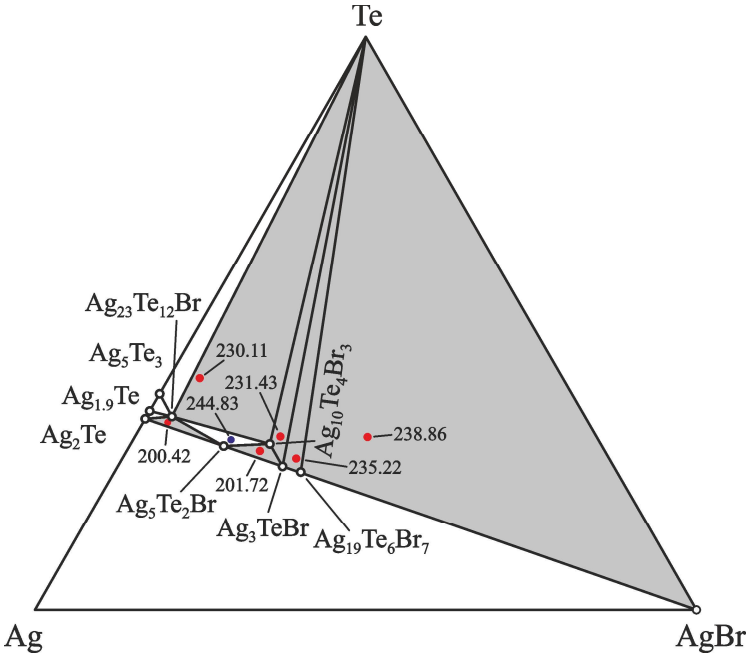

Fig. 2. The phase equilibria of the Ag–Te–Br system in the $AgBr–Ag_2Te–Te$ part, below T = 500 K. Red dots indicate compositions of the positive electrodes of the ECCs in phase regions PR(1)–(6). EMF values (mV) at T=460 K are shown for some phase compositions.

The division of **(I)** is based on reports [5–12] and our investigations of the boundaries of phase fields by EMF method. For instance, three-phase regions that is more distant from the point of silver are characterized by higher EMF value at T=const (Table 2). The correctness of the suggested limits of three-phase regions PR(1)–(6) is confirmed by the following calculations of thermodynamic functions for $Ag_{23}Te_{12}Br$. Phase region PR(7) is characterized by higher EMF value compared to phase region PR(6) that is more distant from the point of silver. This is due to the metastable set of phases in PR(7).

The established division of **(I)** relative to the position of Ag can be used for the calculation of thermodynamic properties of the ternary compounds that are at equilibrium in these regions. The AgBr–$Ag_{19}Te_6Br_7$–Te phase region is the farthest from the point of Ag. For this region, the electrochemical process of the synthesis of the $Ag_{19}Te_6Br_7$ compound from Ag, Te, and AgBr can be expressed as:

$$12Ag = 12Ag^+ + 12e^- \text{ – left electrode (reference system),}$$

$$12Ag^+ + 12e^- + 7AgBr + 6Te = Ag_{19}Te_6Br_7 \text{ – right electrode (sample system),}$$

$$12Ag + 7AgBr + 6Te = Ag_{19}Te_6Br_7 \text{ – overall cell reaction.} \quad (R1)$$

The overall cell reactions in the positive electrodes of ECCs (A) for phase regions PR(2)–(6) can be expressed as:

$$2Ag + Ag_{19}Te_6Br_7 + Te = 7Ag_3TeBr, \quad (R2)$$

$$Ag + 3Ag_3TeBr + Te = Ag_{10}Te_4Br_3, \quad (R3)$$

$$Ag + Ag_{10}Te_4Br_3 = Ag_5Te_2Br + 2Ag_3TeBr, \quad (R4)$$

$$2Ag + Ag_{23}Te_{12}Br = 10Ag_2Te + Ag_5Te_2Br, \quad (R5)$$

$$59Ag + Ag_{10}Te_4Br_3 + 32Te = 3Ag_{23}Te_{12}Br. \quad (R6)$$

Based on reactions (R1)–(R6), the compositions of the PE of the ECCs were determined by the following Ag : Te : AgBr component ratios: 7 : 6 : 7, 13 : 7 : 7, 13 : 8 : 6, 15 : 8 : 6, 23 : 12 : 1, and 17 : 12 : 1, respectively.

Temperature variations of the EMF values of the ECCs with PEs of the PR(1)–(6) are listed in Table 3 and plotted in Fig. 3.

Table 3. The measured values of temperature and EMF of the ECCs from different phase regions of the Ag–Te–Br system [a].

T/K	$E_{(R1)}$/mV	$E_{(R2)}$/mV	$E_{(R3)}$/mV	$E_{(R4)}$/mV	$E_{(R5)}$/mV	$E_{(R6)}$/mV
	PR(1)	PR(2)	PR(3)	PR(4)	PR(5)	PR(6)
440.2	234.72	231.41	228.12	196.03	194.73	226.32
445.2	235.48	232.63	229.21	197.41	196.33	227.28
450.1	236.78	233.24	229.86	198.86	197.49	228.07
455.1	237.98	234.26	230.72	200.56	198.83	229.01
460.0	238.86	235.22	231.43	201.72	200.42	230.11

465.0	239.85	236.27	232.69	203.35	201.66	230.83
469.9	241.22	237.13	233.71	204.59	203.17	231.85
474.8	242.06	238.30	234.27	206.06	204.66	232.57
479.7	243.02	238.96	235.34	207.33	205.83	233.58
484.7	244.39	240.01	236.25	208.91	207.14	234.37
489.6	245.45	240.85	237.28	210.35	208.75	235.09
494.5	246.73	241.83	238.02	211.81	210.16	236.32
499.4	247.65	242.92	238.89	213.25	211.37	237.24
503.3	248.49	243.57	239.63	214.45	212.52	238.05
507.2	249.39	244.39	240.42	215.51	213.69	238.86

[a] Standard uncertainties u are $u(T)$=0.1 K, $u(E)$=0.3 mV.

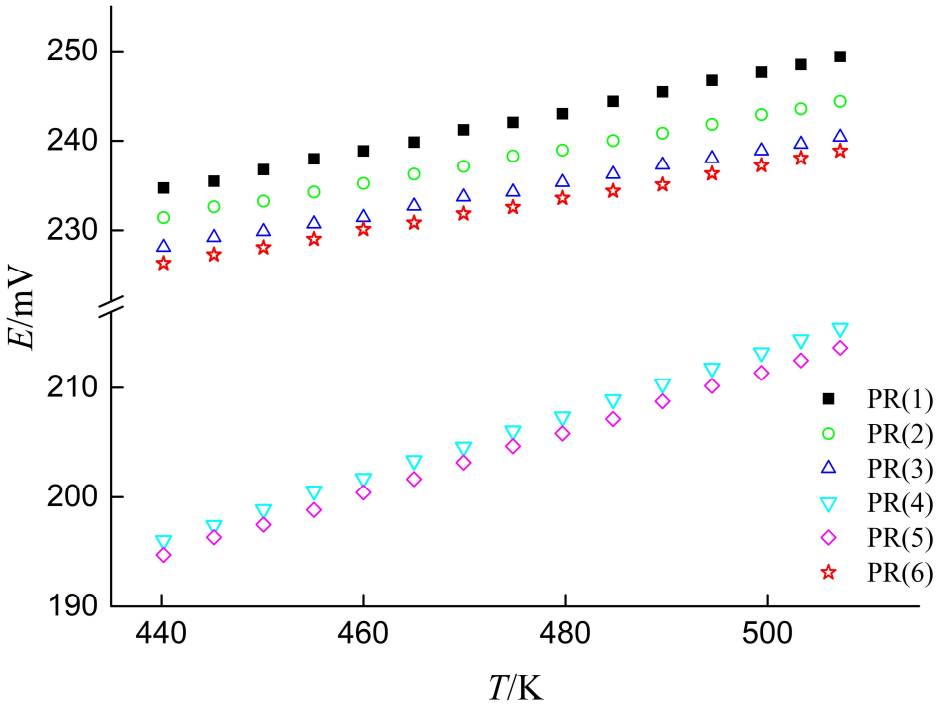

Fig. 3. Temperature dependences of EMF on temperature of the ECCs with the positive electrodes of the phase regions PR(1)–(6).

The treatment of the E vs T dependencies for reactions (R1)–(R6) in the range between T=(440 and 507) K was performed by the least-squares method [16,33,34] using Eq. (1):

$$E = a + bT \equiv \bar{E} + b(T - \bar{T}), \tag{1}$$

where $\bar{E} = \frac{\sum E_i}{n}$, $\bar{T} = \frac{\sum T_i}{n}$ (E_i is the EMF of ECC at temperature T_i; n is number of experimental pairs E_i and T_i).

Coefficients b and a were calculated by the following Eqs. (2) and (3):

$$b = \frac{\sum[(E_i - \bar{E})(T_i - \bar{T})]}{\sum(T_i - \bar{T})^2}, \tag{2}$$

$$a = \bar{E} - b\bar{T}. \tag{3}$$

The statistical dispersions of the measurement uncertainties consisted of the calculation variances of experimental values of EMF E (u_E^2), coefficients b (u_b^2) and a (u_a^2), as well as dispersions of the calculation by Eq. (1), EMF values $\tilde{E}$ ($u_{\tilde{E}}^2$):

$$u_E^2 = \frac{\sum(E_i - \tilde{E}_i)^2}{n-2}, \tag{4}$$

$$u_b^2(T) = \frac{u_E^2}{\sum(T_i - \bar{T})^2}, \tag{5}$$

$$u_a^2(T) = \frac{u_E^2}{n} + \frac{u_E^2 \bar{T}^2}{\sum(T_i - \bar{T})^2}, \tag{6}$$

$$u_{\tilde{E}}^2(T) = \frac{u_E^2}{n} + u_b^2(T_i - \bar{T})^2. \tag{7}$$

Uncertainties (Δ_i) of the corresponding quantities can be calculated by the Eq. (8):

$$\Delta_i = k u_i \tag{8}$$

where k is the Student's coefficient, and u_i is the standard deviation. At the confidence level of 95% and $n = 15$, Student's coefficient is $k = 2.13$ [35].

According to [18,20], the final equation of the E vs T dependences together with the statistical dispersions can be express as:

$$E = a + bT \pm k\sqrt{\left(\frac{u_E^2}{n} + u_b^2(T_i - \bar{T})^2\right)}. \tag{9}$$

Experimental values of the EMF and temperature presented in Table 3 were used to calculate the coefficients and dispersions in Eq. (9) for the PR(1)–(6). Result of calculations is presented in Table 4.

Table 4. Relations between the EMF and temperature for type (A) ECCs in phase regions PR(1)–(6) of the Ag–Te–Br system between T=(440 and 507) K. Values of the coefficients a and b are obtained through linear least squares analysis of the measured E vs T data, n is the number of experimental points, k is Student's coefficient at 95% level of confidence [a].

Phase region	$E = a + bT \pm k\sqrt{\left(\frac{u_E^2}{n} + u_b^2(T_i - \bar{T})^2\right)}$
PR(1)	$E_{(R1)} = 137.17 + 221.17 \cdot 10^{-3}T \pm 2.13\sqrt{\left(\frac{0.019}{15} + 2.88 \cdot 10^{-6}(T_i - 474.58)^2\right)}$
PR(2)	$E_{(R2)} = 146.84 + 192.22 \cdot 10^{-3}T \pm 2.13\sqrt{\left(\frac{0.011}{15} + 1.64 \cdot 10^{-6}(T_i - 474.58)^2\right)}$
PR(3)	$E_{(R3)} = 147.39 + 183.32 \cdot 10^{-3}T \pm 2.13\sqrt{\left(\frac{0.017}{15} + 2.60 \cdot 10^{-6}(T_i - 474.58)^2\right)}$
PR(4)	$E_{(R4)} = 68.05 + 290.71 \cdot 10^{-3}T \pm 2.13\sqrt{\left(\frac{0.009}{15} + 1.31 \cdot 10^{-6}(T_i - 474.58)^2\right)}$

PR(5)	$E_{(R5)} = 70.71 + 281.81 \cdot 10^{-3}T \pm 2.13\sqrt{\left(\frac{0.011}{15} + 1.60 \cdot 10^{-6}(T_i - 474.58)^2\right)}$	
PR(6)	$E_{(R6)} = 144.98 + 184.69 \cdot 10^{-3}T \pm 2.13\sqrt{\left(\frac{0.029}{15} + 4.43 \cdot 10^{-6}(T_i - 474.58)^2\right)}$	

[a] Standard uncertainties u are $u(T)$=0.1 K, $u(E)$=0.3 mV, $u(a)$=0.97, $u(b)$=0.0018.

The Gibbs energy, entropy, and enthalpy of the reactions (R1)–(R6) can be calculated by combining the measured EMF values of each ECCs and the thermodynamic Eqs. (10)–(12) [36,37]:

$$\Delta_r G = -z \cdot \mathrm{F} \cdot E, \quad (10)$$

$$\Delta_r H = -z \cdot \mathrm{F} \cdot [E - (dE/dT) \cdot T], \quad (11)$$

$$\Delta_r S = z \cdot \mathrm{F} \cdot (dE/dT), \quad (12)$$

where z is the number of electrons involved in the reactions (R1)–(R6), F = 96485.33289 C·mol^{-1} is Faraday constant, and E in V is the EMF of the ECCs.

The thermodynamic functions of reactions (R1)–(R6) at T=298 K were calculated using Eqs. (10)–(12) in the approximation $\left(\frac{\partial \Delta_r H}{\partial T}\right)_p = 0$ and $\left(\frac{\partial \Delta_r S}{\partial T}\right)_p = 0$ [31,38]. The results of the calculations are presented in Table 5.

Table 5. Standard thermodynamic values of the reactions (R1)–(R6) in the ECCs[a].

Reaction	$-\Delta_r G^\circ$	$-\Delta_r H^\circ$	$\Delta_r S^\circ$
	kJ·mol^{-1}		J·(mol·K)$^{-1}$
(R1)	235.13 ± 0.74	158.82 ± 1.99	256.08 ± 4.18
(R2)	39.39 ± 0.09	28.34 ± 0.25	37.09 ± 0.53
(R3)	19.49 ± 0.06	14.22 ± 0.16	17.69 ± 0.33
(R4)	14.92 ± 0.04	6.57 ± 0.11	28.05 ± 0.23
(R5)	29.85 ± 0.09	13.65 ± 0.25	54.38 ± 0.52
(R6)	1138.63 ± 3.52	825.32 ± 9.42	1051.37 ± 19.80

[a] Uncertainties for $\Delta_r G^\circ$, $\Delta_r H^\circ$, and $\Delta_r S^\circ$ are standard uncertainties.

Standard Gibbs energy, enthalpy, and entropy of reaction (R1) are related to the Gibbs energy, enthalpy of formation and entropy of compounds and pure elements by the following equations:

$$\Delta_{r(R1)} G^\circ = \Delta_f G^\circ_{Ag_{19}Te_6Br_7} - 7\Delta_f G^\circ_{AgBr}, \quad (13)$$

$$\Delta_{r(R1)} H^\circ = \Delta_f H^\circ_{Ag_{19}Te_6Br_7} - 7\Delta_f H^\circ_{AgBr}, \quad (14)$$

$$\Delta_{r(R1)} S^\circ = S^\circ_{Ag_{19}Te_6Br_7} - 12S^\circ_{Ag} - 7S^\circ_{AgBr} - 6S^\circ_{Te}. \quad (15)$$

It follows from Eqs. (13)–(15) that:

$$\Delta_f G^\circ_{Ag_{19}Te_6Br_7} = 7\Delta_f G^\circ_{AgBr} + \Delta_{r(R1)} G^\circ, \quad (16)$$

$$\Delta_f H^\circ_{Ag_{19}Te_6Br_7} = 7\Delta_f H^\circ_{AgBr} + \Delta_{r(R1)} H^\circ, \quad (17)$$

$$S^\circ_{Ag_{19}Te_6Br_7} = 12S^\circ_{Ag} + 7S^\circ_{AgBr} + 6S^\circ_{Te} + \Delta_{r(R1)} S^\circ. \quad (18)$$

The corresponding reactions to determine $\Delta_f G^\circ$, $\Delta_f H^\circ$, and S° for the Ag_3TeBr, $Ag_{10}Te_4Br_3$, Ag_5Te_2Br, and $Ag_{23}Te_{12}Br$ compounds can be written similar to Eqs. (16)–(18) with their appropriate stochiometric numbers.

Combining Eqs. (10)–(12) and (16)–(18), using thermodynamic data of the pure elements [39], and compounds AgBr [39], Ag_2Te [31], the standard Gibbs energy of formation of compounds of the Ag–Te–Br system were calculated.

$$\Delta_f G^\circ_{Ag_{19}Te_6Br_7}/(\text{kJ·mol}^{-1}) = -(861.9 \pm 3.4) - (175.2 \pm 1.0) \cdot 10^{-3} T/\text{K}, \quad (19)$$

$$\Delta_f G^\circ_{Ag_3TeBr}/(\text{kJ·mol}^{-1}) = -(127.2 \pm 0.5) - (30.5 \pm 0.2) \cdot 10^{-3} T/\text{K}, \quad (20)$$

$$\Delta_f G^\circ_{Ag_{10}Te_4Br_3}/(\text{kJ·mol}^{-1}) = -(395.8 \pm 1.7) - (109.2 \pm 0.7) \cdot 10^{-3} T/\text{K}, \quad (21)$$

$$\Delta_f G^\circ_{Ag_5Te_2Br}/(\text{kJ·mol}^{-1}) = -(148.0 \pm 2.9) - (76.2 \pm 1.6) \cdot 10^{-3} T/\text{K}, \quad (22)$$

$$\Delta_f G^\circ_{Ag_{23}Te_{12}Br}/(\text{kJ·mol}^{-1}) = -(429.2 \pm 18.7) - (326.4 \pm 8.5) \cdot 10^{-3} T/\text{K}, \quad (23)$$

$$\Delta_f G^\circ_{Ag_{23}Te_{12}Br}/(\text{kJ·mol}^{-1}) = -(407.2 \pm 11.1) - (386.7 \pm 9.7) \cdot 10^{-3} T/\text{K}. \quad (24)$$

A comparative summary of the calculated values together with the available literature data is presented in Table 6. The standard uncertainties for the thermodynamic data of this work were calculated by accumulating the calculated deviations in Table 5 and data of Refs. [31,39].

Table 6. Summary of the standard thermodynamic properties of selected phases in the Ag–Te–Br system [a].

Phase	$-\Delta_f G^\circ$	$-\Delta_f H^\circ$	S°	Ref.
	kJ·mol^{-1}		J·(mol·K)$^{-1}$	
Ag	0	0	42.55 ± 0.21	[39]
Te	0	0	49.71 ± 0.20	[39]
Br_2	0	0	152.20 ± 0.30	[39]
AgBr	97.0 ± 0.2	100.4 ± 0.2	107.1 ± 0.4	[39]
Ag_2Te	38.56 ± 0.93	29.49 ± 1.56	165.2 ± 4.1	[31]
Ag_3TeBr	136.1	127.3	–	[14]
Ag_3TeBr	136.3 ± 0.3	127.2 ± 0.5	284.0 ± 1.7	This work
$Ag_{19}Te_6Br_7$	914.1 ± 2.1	861.9 ± 3.4	1814.6 ± 10.7	This work
$Ag_{10}Te_4Br_3$	428.3 ± 1.0	395.7 ± 1.7	961.8 ± 5.8	This work
Ag_5Te_2Br	170.7 ± 1.7	148.0 ± 2.9	464.5 ± 9.7	This work
$Ag_{23}Te_{12}Br$*	526.4 ± 11.1	429.2 ± 18.7	1977.7 ± 51.6	This work
$Ag_{23}Te_{12}Br$**	522.3 ± 4.6	407.0 ± 11.1	2038.1 ± 44.3	This work

[a] Uncertainties for $\Delta_f G^\circ$, $\Delta_f H^\circ$, $T\Delta_f S^\circ$, and S° are standard uncertainties.

* PR(5).

** PR(6).

The Ag_5Te_2Br compound does not exist in equilibrium state under normal conditions [7]. In this study, the compound was obtained in ECCs with PR(4) and (5) by the decomposition of $Ag_{10}Te_4Br_3$ and $Ag_{23}Te_{12}Br$ by Eqs. (R4) and (R5), respectively. The decomposition products of these ternary compounds are the mixtures of the phases Ag_5Te_2Br, Ag_3TeBr and Ag_5Te_2Br, Ag_2Te, respectively. The Ag_5Te_2Br compound preserves its crystal structure in contact with the stable phases Ag_2Te and Ag_3TeBr. Attempts to non-activation synthesis Ag_5Te_2Br in potential-defining processes of the decomposition of $Ag_{10}Te_4Br_3$ and $Ag_{23}Te_{12}Br$ by the reaction

$$7Ag + 5Ag_{10}Te_4Br_3 + Ag_{23}Te_{12}Br = 16Ag_5Te_2Br \quad (R7)$$

were unsuccessful. The EMF value of ECC with positive electrode of PR(7) exceeds in the range of T=(440–500) K the EMF value of the cell with PE of PR(6) that lies farther from Ag (Table 2). It is likely that the products of simultaneous decomposition of $Ag_{10}Te_4Br_3$ and $Ag_{23}Te_{12}Br$ in PR(7) are a thermodynamically non-equilibrium combination of compounds that includes Ag_5Te_2Br, Ag_2Te, and Ag_3TeBr. The metastable set of phases determines the EMF value of the cell.

The $\Delta_f G^\circ$ values of the $Ag_{23}Te_{12}Br$ compound were calculated from the E vs T dependences of two fundamentally different potential-forming processes: the decomposition of $Ag_{23}Te_{12}Br$ into Ag_2Te and Ag_5Te_2Br in PR(5); and the synthesis of $Ag_{23}Te_{12}Br$ from $Ag_{10}Te_4Br_3$ and Ag, Te elements in PR(6). The convergence within the experiment error of the calculated $\Delta_f G^\circ$ values for the $Ag_{23}Te_{12}Br$ compound (the relative difference is less than 1%) serves as the validation of:

a) phase composition and division of the equilibrium concentration space **(I)**;
b) calculated values of the thermodynamic functions of the $Ag_{19}Te_6Br_7$, Ag_3TeBr, $Ag_{10}Te_4Br_3$, and Ag_5Te_2Br compounds;
c) reliability of the literature values of the thermodynamic properties of AgBr, Ag_2Te, and Ag_3TeBr.

4. Conclusions

The division of the concentration space of the AgBr–Ag_2Te–Te system **(I)** into 10 three-phase regions was proposed. The positions of the phase regions AgBr–$Ag_{19}Te_6Br_7$–Te, $Ag_{19}Te_6Br_7$–Ag_3TeBr–Te, Ag_3TeBr–$Ag_{10}Te_4Br_3$–Te, Ag_3TeBr–Ag_5Te_2Br–$Ag_{10}Te_4Br_3$, Ag_5Te_2Br–Ag_2Te–$Ag_{23}Te_{12}Br$, and $Ag_{10}Te_4Br_3$–$Ag_{23}Te_{12}Br$–Te vs the point of Ag were used to write equations of overall cell reactions.

Low-temperature (T≤500 K) non-activation synthesis of the equilibrium set of phases from metastable powder mixture of Ag, Te, and AgBr was carried out in the R(Ag^+) region of the positive electrode of the electrochemical cell adjacent to the solid electrolyte. The ratios of Ag, Te, and AgBr were determined based on the equations of the overall cell reactions. The R(Ag^+) region

is characterized by a positive spatial charge from the Ag^+ ions, migrated from the left electrode for thermodynamic reasons. The silver cations play the role of a small nucleus of the stable phase. The described non-activation synthesis of compounds makes possible the determination of the phase composition of inorganic systems in the part of the *T*–*x* space where the energy of the oscillating motion of atoms is insufficient for the formation of the nucleation centers of phases.

Equations of temperature dependences of Gibbs energies of formation of ternary compounds were obtained from EMF vs *T* dependences of ECCs, and $\Delta_f G^\circ$, $\Delta_f H^\circ$, $T\Delta_f S^\circ$, and S° values were calculated. The criterion of the validity of obtained values of thermodynamic functions of the ternary compounds of system **(I)** is the agreement, within the experiment error, of $\Delta_f G^\circ$ values of the $Ag_{23}Te_{12}Br$ compound that were calculated from the phase regions Ag_5Te_2Br–Ag_2Te–$Ag_{23}Te_{12}Br$ and $Ag_{10}Te_4Br_3$–$Ag_{23}Te_{12}Br$–Te.

Data on thermodynamic properties of the compounds may be used in CALPHAD modeling of four-element and more complex phase space of the Ag–{Se, Te}–{Cl, Br, I} systems to determine compositions with maximum values of thermoelectric efficiency *ZT*.

Declaration of Competing Interest

The authors declare that there are no conflicts of interest.

CRediT author statement

Mykola Moroz: Conceptualization, Methodology, Investigation, Writing - Review & Editing
Fiseha Tesfaye: Conceptualization, Methodology, Writing - Review & Editing
Pavlo Demchenko: Investigation, Data Curation, Writing - Original Draft
Myroslava Prokhorenko: Data Curation, Writing - Original Draft
Serhiy Prokhorenko: Data Curation, Writing - Review & Editing
Oleksandr Reshetnyak: Conceptualization, Methodology, Writing - Review & Editing, Supervision

Acknowledgments

This research was supported by the national projects of the Ministry of Education and Science of Ukraine: “Synthesis, physico-chemical and thermodynamic properties of nanosized and nanostructured materials for electrochemical systems” (No. 0120U102184) and “Universal measuring complexes for electrochemical, corrosion and electro-analytical researches” (No. 0119U002208). This work was also supported by the Academy of Finland project (Decision number 311537), as part of the activities of the Johan Gadolin Process Chemistry Centre at Åbo Akademi University.

References

1. S. Chu, A. Majumdar, Opportunities and challenges for a sustainable energy future, Nature. 488 (2012) 294–303. https://doi.org/10.1038/nature11475
2. W. Liu, J. Hu, S. Zhang, M. Deng, C.-G. Han, Y. Liu, New trends, strategies and opportunities in thermoelectric materials: A perspective, Materials Today Physics. 1 (2017) 50–60. https://doi.org/10.1016/j.mtphys.2017.06.001
3. Y. Shi, C. Sturm, H. Kleinke, Chalcogenides as thermoelectric materials, J. Solid State Chem. 270 (2019) 273–279. https://doi.org/10.1016/j.jssc.2018.10.049
4. T. Nilges, S. Lange, M. Bawohl, J.M. Deckwart, M. Janssen, H.-D. Wiemhöfer, R. Decourt, B. Chevalier, J. Vannahme, H. Eckert, R. Weihrich, Reversible switching between p- and n-type conduction in the semiconductor $Ag_{10}Te_4Br_3$, Nature Mater. 8 (2009) 101–108. https://doi.org/10.1038/nmat2358
5. T. Nilges, M. Julia, The Solid Solutions $M_{19}Q_6X_7$ with M = Ag, Cu; Q = S, Se, Te and X = S, Se, Te, Z. Anorg. Allg. Chem. 634 (2008) 2185–2190. https://doi.org/10.1002/zaac.200800128
6. R. Blachnik, H.A. Dreisbach, The phase diagrams of Ag_2X-AgY (X = S, Se, Te; Y = Cl, Br, I): mixtures and the structure of Ag_5Te_2Cl, J. Solid State Chem. 60 (1985) 115–122. https://doi.org/10.1016/0022-4596(85)90171-9
7. J. Messel, T. Nilges, Structure Chemical Aspects of Silver(I) Chalcogenide Halides and Preparation of the x = 1 Member of the Solid Solution $Ag_5Te_2Cl_{1-x}Br_x$, Z. Naturforsch. B. 63 (2008) 1077–1082. https://doi.org/10.1515/znb-2008-0910
8. N. Eckstein, T. Nilges, R. Decourt, J.-L. Bobet, B. Chevalier, Effects of partial anion substitution on the thermoelectric properties of silver(I) chalcogenide halides in the system Ag_5Q_2X with Q=Te, Se and S and X=Br and Cl, J. Solid State Chem. 184 (2011) 778–785. https://doi.org/10.1016/j.jssc.2011.01.031
9. S. Lange, T. Nilges, $Ag_{10}Te_4Br_3$: A New Silver(I) (poly)Chalcogenide Halide Solid Electrolyte, Chem. Mater. 18 (2006) 2538–2544. https://doi.org/10.1021/cm060226m
10. T. Nilges, O. Osters, M. Bawohl, J.-L. Bobet, B. Chevalier, R. Decourt, R. Weihrich, Reversible Property Switching, Thermoelectric Performance, and d10−d10 Interactions in Ag_5Te_2Cl, Chem. Mater. 22 (2010) 2946–2954. https://doi.org/10.1021/cm100269a
11. S. Lange, M. Bawohl, T. Nilges, Crystal Structures and Thermal and Electrical Properties of the New Silver (poly)Chalcogenide Halides $Ag_{23}Te_{12}Cl$ and $Ag_{23}Te_{12}Br$, Inorg. Chem. 47 (2008) 2625–2633. https://doi.org/10.1021/ic701988u
12. O. Osters, T. Nilges, Partial Anion Exchange in $Ag_{23}Te_{12}X$: The Solid Solutions $Ag_{23}Te_{12}Cl_{1-x}Br_x$, $Ag_{23}Te_{12}Br_{1-y}I_y$ and $Ag_{23}Te_{12}Cl_{1-z}I_z$, Z. Anorg. Allg. Chem. 636 (2010) 297–304. https://doi.org/10.1002/zaac.200900294
13. J.-S. Rhyee, K.H. Lee, S.M. Lee, E. Cho, S.I. Kim, E. Lee, Y.S. Kwon, J.H. Shim, G. Kotliar, Peierls distortion as a route to high thermoelectric performance in $In_4Se_{3-\delta}$ crystals, Nature. 459 (2009) 965–968. https://doi.org/10.1038/nature08088
14. M.V. Moroz, M.V. Prokhorenko, P.Yu. Demchenko, Thermodynamic properties of the intermediate phases of a Ag-Te-AgBr system, Russ. J. Phys. Chem. A. 87 (2013) 6–9. https://doi.org/10.1134/S0036024413010147
15. A. Kroupa, Modelling of phase diagrams and thermodynamic properties using Calphad method – Development of thermodynamic databases, Comput. Mater. Sci. 66 (2013) 3–13. https://doi.org/10.1016/j.commatsci.2012.02.003

16. M. Babanly, Y. Yusibov, N. Babanly, The EMF method with solid-state electrolyte in the thermodynamic investigation of ternary copper and silver chalcogenides, in: S. Kara (Ed.), Electromotive Force and Measurement in Several Systems, InTech, 2011: pp. 57–78. https://doi.org/10.5772/28934
17. V.P. Vassiliev, V.A. Lysenko, A New Approach for the Study of Thermodynamic Properties of Lanthanide Compounds, Electrochimica Acta. 222 (2016) 1770–1777. https://doi.org/10.1016/j.electacta.2016.11.075
18. N.B. Babanly, E.N. Orujlu, S.Z. Imamaliyeva, Y.A. Yusibov, M.B. Babanly, Thermodynamic investigation of silver-thallium tellurides by EMF method with solid electrolyte Ag_4RbI_5, J. Chem. Thermodyn. 128 (2019) 78–86. https://doi.org/10.1016/j.jct.2018.08.012
19. M.B. Babanly, L.F. Mashadiyeva, D.M. Babanly, S.Z. Imamaliyeva, D.B. Tagiev, Yu.A. Yusibov, Some Issues of Complex Studies of Phase Equilibria and Thermodynamic Properties in Ternary Chalcogenide Systems Involving Emf Measurements (Review), Russ. J. Inorg. Chem. 64 (2019) 1649–1671. https://doi.org/10.1134/S0036023619130035
20. S.Z. Imamaliyeva, S.S. Musayeva, D.M. Babanly, Y.I. Jafarov, D.B. Taghiyev, M.B. Babanly, Determination of the thermodynamic functions of bismuth chalcoiodides by EMF method with morpholinium formate as electrolyte, Thermochim. Acta. 679 (2019) 178319. https://doi.org/10.1016/j.tca.2019.178319
21. I. Santoso, P. Taskinen, A. Jokilaakso, D. Lindberg, Thermodynamic properties of Ag–Au alloys measured by a solid-state electrolyte EMF method, Thermochim. Acta. 689 (2020) 178658. https://doi.org/10.1016/j.tca.2020.178658
22. E. Robinel, B. Carette, M. Ribes, Silver sulfide based glasses (I): glass forming regions, structure and ionic conduction of glasses in GeS_2–Ag_2S and GeS_2–Ag_2S–AgI systems, J. Non-Cryst. Solids. 57 (1983) 49–58. https://doi.org/10.1016/0022-3093(83)90407-6
23. M.V. Moroz, P.Y. Demchenko, S.V. Prokhorenko, V.M. Moroz, Physical properties of glasses in the Ag_2GeS_3-AgBr system, Phys. Solid State. 55 (2013) 1613–1618. https://doi.org/10.1134/S1063783413080209
24. M.V. Moroz, P.Yu. Demchenko, O.G. Mykolaychuk, L.G. Akselrud, R.E. Gladyshevskii, Synthesis and electrical conductivity of crystalline and glassy alloys in the Ag_3GeS_3Br-GeS_2 system, Inorg. Mater. 49 (2013) 867–871. https://doi.org/10.1134/S0020168513090100
25. M. Moroz, F. Tesfaye, P. Demchenko, M. Prokhorenko, D. Lindberg, O. Reshetnyak, L. Hupa, Determination of the thermodynamic properties of the $Ag_2CdSn_3S_8$ and Ag_2CdSnS_4 phases in the Ag–Cd–Sn–S system by the solid-state electrochemical cell method, J. Chem. Thermodyn. 118 (2018) 255–262. https://doi.org/10.1016/j.jct.2017.12.001
26. M.V. Moroz, M.V. Prokhorenko, P.Yu. Demchenko, O.V. Reshetnyak, Thermodynamic properties of saturated solid solutions of Ag_7SnSe_5Br and Ag_8SnSe_6 compounds in the Ag–Sn–Se–Br system measured by the EMF method, J. Chem. Thermodyn. 106 (2017) 228–231. https://doi.org/10.1016/j.jct.2016.12.004
27. M.V. Moroz, P.Yu. Demchenko, M.V. Prokhorenko, O.V. Reshetnyak, Thermodynamic Properties of Saturated Solid Solutions of the Phases Ag_2PbGeS_4, $Ag_{0.5}Pb_{1.75}GeS_4$ and $Ag_{6.72}Pb_{0.16}Ge_{0.84}S_{5.20}$ of the Ag-Pb-Ge-S System Determined by EMF Method, J. Phase Equilib. Diffus. 38 (2017) 426–433. https://doi.org/10.1007/s11669-017-0563-6
28. F. Tesfaye, P. Taskinen, Electrochemical study of the thermodynamic properties of matildite (β-AgBiS2) in different temperature and compositional ranges, J. Solid State Electrochem. 18 (2014) 1683–1694. https://doi.org/10.1007/s10008-014-2395-1

29. M.V. Moroz, M.V. Prokhorenko, B.P. Rudyk, Thermodynamic properties of phases of the Ag-Ge-Te system, Russ. J. Electrochem. 50 (2014) 1177–1181. https://doi.org/10.1134/S1023193514120039
30. M.V. Moroz, M.V. Prokhorenko, S.V. Prokhorenko, Determination of thermodynamic properties of Ag_3SBr superionic phase using EMF technique, Russ. J. Electrochem. 51 (2015) 886–889. https://doi.org/10.1134/S1023193515090098
31. M.V. Voronin, E.G. Osadchii, E.A. Brichkina, Thermochemical properties of silver tellurides including empressite (AgTe) and phase diagrams for Ag–Te and Ag–Te–O, Phys. Chem. Miner. 44 (2017) 639–653. https://doi.org/10.1007/s00269-017-0889-y
32. Karapetyants M.Kh. The Chemical thermodynamics. Moscow, Goskhimizdat. 1953. [in Russian]
33. A.J. Gordon, R.A. Ford, The Chemist's Companion: A Handbook of Practical Data, Techniques, and References, Wiley, New York, 1972.
34. A.G. Morachevsky, G.F. Voronin, V.A. Geiderich, I.B. Kutsenok Electrochemical methods of research in the thermodynamics of metal systems. Academic Book. 2003.
35. F.J. Gravetter, L.B. Wallnau, Statistics for the behavioral sciences, 10th edition, Cengage Learning, Australia ; United States, 2017.
36. E.G. Osadchii, O.A. Rappo, Determination of standard thermodynamic properties of sulfides in the Ag-Au-S system by means of a solid-state galvanic cell, Am. Mineral. 89 (2004) 1405–1410. https://doi.org/10.2138/am-2004-1007
37. E.G. Osadchii, E.A. Echmaeva, The system Ag-Au-Se: Phase relations below 405 K and determination of standard thermodynamic properties of selenides by solid-state galvanic cell technique, Am. Mineral. 92 (2007) 640–647. https://doi.org/10.2138/am.2007.2209
38. M.V. Voronin, E.G. Osadchii, Thermodynamic properties of silver and bismuth sulfosalt minerals, pavonite ($AgBi_3S_5$) and matildite ($AgBiS_2$) and implications for ore deposits, Economic Geology. 108 (2013) 1203–1210. https://doi.org/10.2113/econgeo.108.5.1203.
39. R.A. Robie, B.S. Hemingway, Thermodynamic properties of minerals and related substances at 298.15 K and 1 bar (10^5 pascals) pressure and at higher temperatures, U.S. Geological Survey Bulletin, Washington, 1995. https://doi.org/10.3133/b2131